A New Technique of Indirect Component Mode Synthesis and Model Test Validation for Truss Bridge Modal Analysis

Kai-liang Lu, Wei Yan, Qiu-yi Ding and Chao Wang

Logistics Engineering College, Shanghai Maritime University, Shanghai 201306, China
lkl1984@163.com

Abstract

A new technique of dual-compatibilities free-interface component mode synthesis (CMS) was derived by transforming link substructure into super element with Guyan static condensation. The new CMS technique has high calculation accuracy, can efficiently reduce degree of freedom (DOF) of the system, thus, it has a widespread application prospect in dynamic analysis of the structures containing nonlinear link components such as Lead Rubber Bearing (LRB), nonlinear spring, etc. Based on the new CMS technique and the general free-interface CMS method, the inherent characteristics of a truss bridge, rigid or LRB linked, in the Automatic Container Terminal (ACT), was compared. The results show that LRB has obvious effect on truss bridge structural frequency modulation. Structural dynamic model similarity principle with respect to inherent characteristics is achieved with dimensional analysis method. Accordingly, a miniature model for the truss bridge is designed to test frequency response by the hammer method. The results of model test and prototype simulation prove with each other, that the simulation results and the test design are reliable, also validates the proposed CMS technique and the LRB's effect on frequency modulation.

Keywords: *Free-interface Component Mode Synthesis (CMS), Link Substructure, Modal Analysis, Truss Bridge, Structural Model Test*

1. Introduction

As one of the most effectual methods for modern large and complex structural dynamics analysis, component mode synthesis (CMS) has been used in the dynamic analysis of structural fields, such as aerospace, ships, vehicles, nuclear power, civil construction, *etc.* [1-3]. Among lots of different CMS methods, the free-interface CMS method has been the most widely used and constantly improved due to its advantages such as no interface DOFs in synthesized equation, high computational efficiency and convenience to validate with experimental modal analysis technology [4-6].

Some researchers proposed the concept of link substructure. The feature definition of link substructure in CMS has been presented, namely, only the interface DOF without internal DOF, and all the interface DOF shared with non-link substructures [5, 6]. The indirect mixed-interface CMS method is also raised and the two link ways of displacement coordination and dual coordination of both displacement and force are discussed.

In the CMS methods, as long as the master DOFs are interface coordinates only, it is named as the super-element method. The commonly used super-element methods include Guyan static condensation, Kuhar fixed-frequency dynamic condensation and variable-frequency dynamic condensation [7].

According to the definition, link substructure is essentially a kind of static or dynamic transformed super element. Based on this, this paper takes link substructure as super element to deduce the free-interface component mode synthesis technique with link substructure as super-element (referred to as super-element indirect CMS), and applies this technique to the modal analysis of a truss bridge, of which the girder and brace are lead rubber bearings (LRB) linked or rigid linked, in the automated container terminal (ACT) [8]. Moreover, the simulation results are verified through structural model test.

2. Super-element Indirect CMS by Guyan Static Condensation

2.1 Substructure Division

Yet the general, discuss the case of a link substructure between two free-interface substructures, as shown in Figure 1. All the interface DOF of substructure E are shared with adjacent substructures A and B. ${}^{A}\boldsymbol{u}_j$, ${}^{B}\boldsymbol{u}_j$ are respectively the interface DOF of substructure A and B; ${}^{E}\boldsymbol{u}_{jA}$, ${}^{E}\boldsymbol{u}_{jB}$ are respectively the communal interface DOF that substructure E shares with substructure A and B, apparently, ${}^{E}\boldsymbol{u}_m = \left[{}^{E}\boldsymbol{u}_{jA} \quad {}^{E}\boldsymbol{u}_{jB} \right]^{\mathrm{T}}$. ${}^{A}\boldsymbol{f}_j$, ${}^{B}\boldsymbol{f}_j$ are respectively the interface-force vectors that substructure A and B work on their respective interface DOF; ${}^{E}\boldsymbol{f}_{jA}$, ${}^{E}\boldsymbol{f}_{jB}$ are respectively the interface-force vectors that substructure E work on interface DOF *jA* and *jB*.

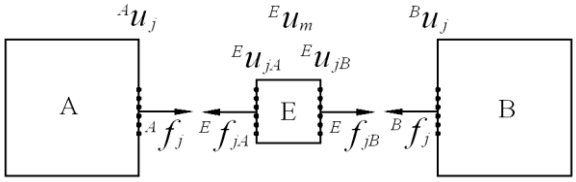

Figure 1. Sketch map of substructure interface connection

2.2 The first coordinate transformation for substructures

2.2.1 Free-interface substructure

Set the stiffness matrix and mass matrix of substructure A in physical coordinates as

$$ {}^{\mathrm{A}}\boldsymbol{z} = \begin{bmatrix} {}^{\mathrm{A}}\boldsymbol{z}_{ii} & {}^{\mathrm{A}}\boldsymbol{z}_{ij} \\ {}^{\mathrm{A}}\boldsymbol{z}_{ji} & {}^{\mathrm{A}}\boldsymbol{z}_{jj} \end{bmatrix}, \quad \boldsymbol{z} = \boldsymbol{k}, \boldsymbol{m} \tag{1} $$

Where, subscript *i* denote substructure's non-interface DOFs and *j* denotes substructure's interface DOFs. Substructure B is also an free-interface substructure. Corresponding matrix of substructure B can be obtained by changing left superscript ^{A} to ^{B}. We can omit the left superscript in the following deduction.

Use the assumed branch mode set $\boldsymbol{\Phi}$, composed of first-*k*-order normal modes $\boldsymbol{\Phi}_k$ and residual attachment modes $\boldsymbol{\Psi}_d$, as the transformation matrix, thus the transformation relation between physical coordinate $\boldsymbol{u}$ and modal coordinate $\boldsymbol{p}$ is

$$ \boldsymbol{u} = \begin{Bmatrix} \boldsymbol{u}_i \\ \boldsymbol{u}_j \end{Bmatrix} = \begin{bmatrix} \boldsymbol{\Phi}_{ik} & \boldsymbol{\Psi}_{id} \\ \boldsymbol{\Phi}_{jk} & \boldsymbol{\Psi}_{jd} \end{bmatrix} \begin{Bmatrix} \boldsymbol{p}_k \\ \boldsymbol{f}_j \end{Bmatrix} = \boldsymbol{\Phi p} \tag{2} $$

Where, $\boldsymbol{f}_j$ is the interface-force vector that substructure works on interface DOF *j*. The calculation of residual attachment modes $\boldsymbol{\Psi}_d$ considering substructure's rigid body mode or not can refer to Literature [9].

Through the regularization of mode to mass matrix, the stiffness matrix and mass matrix of free-interface substructure in modal coordinates can be derived as

$$\bar{\boldsymbol{m}} = \begin{bmatrix} \boldsymbol{I}_{kk} & \\ & \boldsymbol{\Psi}_d^{\mathrm{T}} \boldsymbol{m} \boldsymbol{\Psi}_d \end{bmatrix} \qquad \bar{\boldsymbol{k}} = \begin{bmatrix} \boldsymbol{\Lambda}_{kk} & \\ & \boldsymbol{\Psi}_d^{\mathrm{T}} \boldsymbol{k} \boldsymbol{\Psi}_d \end{bmatrix} \tag{3a)(3b}$$

2.2.2 Super-element link substructure

Super element is characterized by contracting all of substructure's DOFs on interface DOFs (the master DOF) ${}^{E}\boldsymbol{u}_m$. Set the stiffness and mass matrixes of link substructure under master coordinate ${}^{E}\boldsymbol{u}_m$ and slave coordinate ${}^{E}\boldsymbol{u}_s$ as

$${}^{\mathrm{E}}\boldsymbol{z} = \begin{bmatrix} {}^{\mathrm{E}}\boldsymbol{z}_{ss} & {}^{\mathrm{E}}\boldsymbol{z}_{sm} \\ {}^{\mathrm{E}}\boldsymbol{z}_{ms} & {}^{\mathrm{E}}\boldsymbol{z}_{mm} \end{bmatrix}, \quad \boldsymbol{z} = \boldsymbol{m}, \boldsymbol{k} \tag{4}$$

By Guyan static condensation, the stiffness and mass matrixes only under interface DOFs are

$${}^{\mathrm{E}}\tilde{\boldsymbol{z}} = {}^{\mathrm{E}}\boldsymbol{\Psi}_c^{\mathrm{T}} \, {}^{\mathrm{E}}\boldsymbol{z} \, {}^{\mathrm{E}}\boldsymbol{\Psi}_c, \quad \boldsymbol{z} = \boldsymbol{m}, \boldsymbol{k} \tag{5}$$

In which, ${}^{E}\boldsymbol{\Psi}_c$ is static transformation matrix.

$${}^{E}\boldsymbol{\Psi}_c = \begin{bmatrix} -{}^{E}\boldsymbol{k}_{ss}^{-1} \, {}^{E}\boldsymbol{k}_{sm} & \boldsymbol{I} \end{bmatrix}^{\mathrm{T}} \tag{6}$$

Since ${}^{E}\boldsymbol{u}_m = \begin{bmatrix} {}^{E}\boldsymbol{u}_{jA} & {}^{E}\boldsymbol{u}_{jB} \end{bmatrix}^{\mathrm{T}}$, Equation (5) can be written in block form:

$${}^{\mathrm{E}}\tilde{\boldsymbol{z}} = \begin{bmatrix} {}^{\mathrm{E}}\tilde{\boldsymbol{z}}_{(jA)(jA)} & {}^{\mathrm{E}}\tilde{\boldsymbol{z}}_{(jA)(jB)} \\ {}^{\mathrm{E}}\tilde{\boldsymbol{z}}_{(jB)(jA)} & {}^{\mathrm{E}}\tilde{\boldsymbol{z}}_{(jB)(jB)} \end{bmatrix}, \quad \boldsymbol{z} = \boldsymbol{m}, \boldsymbol{k} \tag{7}$$

2.3 Assemble system equation and the second coordinate transformation

2.3.1 Coordination of interface displacement

After the first coordinate transformation, the system's non-damping vibration equation, under the coordinate $\boldsymbol{p} = \begin{bmatrix} {}^{A}\boldsymbol{p}_k & {}^{A}\boldsymbol{f}_j & {}^{E}\boldsymbol{u}_{jA} & {}^{E}\boldsymbol{u}_{jB} & {}^{B}\boldsymbol{p}_k & {}^{B}\boldsymbol{f}_j \end{bmatrix}^{\mathrm{T}}$, is

$$\boldsymbol{m}\ddot{\boldsymbol{p}} + \boldsymbol{k}\boldsymbol{p} = \boldsymbol{0} \tag{8}$$

Where,

$$\boldsymbol{m} = \begin{bmatrix} {}^{\mathrm{A}}\boldsymbol{I}_{kk} & & & & & \\ & {}^{\mathrm{A}}\boldsymbol{\Psi}_d^{\mathrm{T}} \, {}^{\mathrm{A}}\boldsymbol{m} \, {}^{\mathrm{A}}\boldsymbol{\Psi}_d & & & & \\ & & {}^{\mathrm{E}}\tilde{\boldsymbol{m}}_{(jA)(jA)} & {}^{\mathrm{E}}\tilde{\boldsymbol{m}}_{(jA)(jB)} & & \\ & & {}^{\mathrm{E}}\tilde{\boldsymbol{m}}_{(jB)(jA)} & {}^{\mathrm{E}}\tilde{\boldsymbol{m}}_{(jB)(jB)} & & \\ & & & & {}^{\mathrm{B}}\boldsymbol{I}_{kk} & \\ & & & & & {}^{\mathrm{B}}\boldsymbol{\Psi}_d^{\mathrm{T}} \, {}^{\mathrm{B}}\boldsymbol{m} \, {}^{\mathrm{B}}\boldsymbol{\Psi}_d \end{bmatrix} \tag{9a}$$

$$\boldsymbol{k}=\begin{bmatrix} {}^{\mathrm{A}}\boldsymbol{\Lambda}_{kk} & & & & & & \\ & {}^{\mathrm{A}}\boldsymbol{\Psi}_d^{\mathrm{T}}\,{}^{\mathrm{A}}\boldsymbol{k}\,{}^{\mathrm{A}}\boldsymbol{\Psi}_d & & & & & \\ & & {}^{\mathrm{E}}\tilde{\boldsymbol{k}}_{(jA)(jA)} & {}^{\mathrm{E}}\tilde{\boldsymbol{k}}_{(jA)(jB)} & & & \\ & & {}^{\mathrm{E}}\tilde{\boldsymbol{k}}_{(jB)(jA)} & {}^{\mathrm{E}}\tilde{\boldsymbol{k}}_{(jB)(jB)} & & & \\ & & & & {}^{\mathrm{B}}\boldsymbol{\Lambda}_{kk} & & \\ & & & & & {}^{\mathrm{B}}\boldsymbol{\Psi}_d^{\mathrm{T}}\,{}^{\mathrm{B}}\boldsymbol{k}\,{}^{\mathrm{B}}\boldsymbol{\Psi}_d \end{bmatrix} \tag{9b}$$

Since the super-element link substructure E doesn't have non-interface DOF, and its interface DOFs are shared with adjacent free-interface substructure A and B, the coordination conditions of interface displacement can be described as

$${}^{\mathrm{E}}\boldsymbol{u}_{jA}={}^{\mathrm{A}}\boldsymbol{u}_j,\ {}^{\mathrm{E}}\boldsymbol{u}_{jB}={}^{\mathrm{B}}\boldsymbol{u}_j \tag{10a)(10b}$$

On the basis of Equation (10), carry out Equation (2) according to the second line, we obtain

$$\begin{Bmatrix} {}^{E}\boldsymbol{u}_{jA} \\ {}^{E}\boldsymbol{u}_{jB} \end{Bmatrix}=\begin{bmatrix} {}^{A}\boldsymbol{\Phi}_{jk} & \boldsymbol{0} & {}^{A}\boldsymbol{\Psi}_{jd} & \boldsymbol{0} \\ \boldsymbol{0} & {}^{B}\boldsymbol{\Phi}_{jk} & \boldsymbol{0} & {}^{B}\boldsymbol{\Psi}_{jd} \end{bmatrix}\begin{Bmatrix} {}^{A}\boldsymbol{p}_k \\ {}^{B}\boldsymbol{p}_k \\ {}^{A}\boldsymbol{f}_j \\ {}^{B}\boldsymbol{f}_j \end{Bmatrix}=\boldsymbol{T}_1\begin{Bmatrix} {}^{A}\boldsymbol{p}_k \\ {}^{B}\boldsymbol{p}_k \\ {}^{A}\boldsymbol{f}_j \\ {}^{B}\boldsymbol{f}_j \end{Bmatrix} \tag{11}$$

Thus, can achieve

$$\begin{Bmatrix} {}^{A}\boldsymbol{p}_k \\ {}^{A}\boldsymbol{f}_j \\ {}^{E}\boldsymbol{u}_{jA} \\ {}^{E}\boldsymbol{u}_{jB} \\ {}^{B}\boldsymbol{p}_k \\ {}^{B}\boldsymbol{f}_j \end{Bmatrix}=\begin{bmatrix} \boldsymbol{I} & \boldsymbol{0} & \boldsymbol{0} & \boldsymbol{0} \\ \boldsymbol{0} & \boldsymbol{0} & \boldsymbol{I} & \boldsymbol{0} \\ {}^{A}\boldsymbol{\Phi}_{jk} & \boldsymbol{0} & {}^{A}\boldsymbol{\Psi}_{jd} & \boldsymbol{0} \\ \boldsymbol{0} & {}^{B}\boldsymbol{\Phi}_{jk} & \boldsymbol{0} & {}^{B}\boldsymbol{\Psi}_{jd} \\ \boldsymbol{0} & \boldsymbol{I} & \boldsymbol{0} & \boldsymbol{0} \\ \boldsymbol{0} & \boldsymbol{0} & \boldsymbol{0} & \boldsymbol{I} \end{bmatrix}\begin{Bmatrix} {}^{A}\boldsymbol{p}_k \\ {}^{B}\boldsymbol{p}_k \\ {}^{A}\boldsymbol{f}_j \\ {}^{B}\boldsymbol{f}_j \end{Bmatrix}=\boldsymbol{T}_2\begin{Bmatrix} {}^{A}\boldsymbol{p}_k \\ {}^{B}\boldsymbol{p}_k \\ {}^{A}\boldsymbol{f}_j \\ {}^{B}\boldsymbol{f}_j \end{Bmatrix} \tag{12}$$

2.3.2 Coordination of interface force

The static equilibrium equation of link substructure E is given by

$$\begin{Bmatrix} {}^{\mathrm{E}}\boldsymbol{f}_{jA} \\ {}^{\mathrm{E}}\boldsymbol{f}_{jB} \end{Bmatrix}=\begin{bmatrix} {}^{\mathrm{E}}\tilde{\boldsymbol{k}}_{(jA)(jA)} & {}^{\mathrm{E}}\tilde{\boldsymbol{k}}_{(jA)(jB)} \\ {}^{\mathrm{E}}\tilde{\boldsymbol{k}}_{(jB)(jA)} & {}^{\mathrm{E}}\tilde{\boldsymbol{k}}_{(jB)(jB)} \end{bmatrix}\begin{Bmatrix} {}^{\mathrm{E}}\boldsymbol{u}_{jA} \\ {}^{\mathrm{E}}\boldsymbol{u}_{jB} \end{Bmatrix} \tag{13}$$

From Equation (11) and Equation (13), can obtain

$$\begin{Bmatrix} {}^{\mathrm{E}}\boldsymbol{f}_{jA} \\ {}^{\mathrm{E}}\boldsymbol{f}_{jB} \end{Bmatrix}=\begin{bmatrix} {}^{\mathrm{E}}\tilde{\boldsymbol{k}}_{(jA)(jA)} & {}^{\mathrm{E}}\tilde{\boldsymbol{k}}_{(jA)(jB)} \\ {}^{\mathrm{E}}\tilde{\boldsymbol{k}}_{(jB)(jA)} & {}^{\mathrm{E}}\tilde{\boldsymbol{k}}_{(jB)(jB)} \end{bmatrix}\boldsymbol{T}_1\begin{bmatrix} {}^{\mathrm{A}}\boldsymbol{p}_k & {}^{\mathrm{B}}\boldsymbol{p}_k & {}^{\mathrm{A}}\boldsymbol{f}_j & {}^{\mathrm{B}}\boldsymbol{f}_j \end{bmatrix}^{\mathrm{T}} \tag{14}$$

Then, according to the equilibrium conditions of interface force

$${}^{E}\boldsymbol{f}_{jA}=-{}^{A}\boldsymbol{f}_j\quad {}^{E}\boldsymbol{f}_{jB}=-{}^{B}\boldsymbol{f}_j \tag{15a)(15b}$$

And from Equation (14) and Equation (15), can obtain

$$\begin{bmatrix} {}^{E}\tilde{\boldsymbol{k}}_{(jA)(jA)}\,{}^{A}\boldsymbol{\Phi}_{jk} & {}^{E}\tilde{\boldsymbol{k}}_{(jA)(jB)}\,{}^{B}\boldsymbol{\Phi}_{jk} & {}^{E}\tilde{\boldsymbol{k}}_{(jA)(jA)}\,{}^{A}\boldsymbol{\Psi}_{jd}+\boldsymbol{I} & {}^{E}\tilde{\boldsymbol{k}}_{(jA)(jB)}\,{}^{B}\boldsymbol{\Psi}_{jd} \\ {}^{E}\tilde{\boldsymbol{k}}_{(jB)(jA)}\,{}^{A}\boldsymbol{\Phi}_{jk} & {}^{E}\tilde{\boldsymbol{k}}_{(jB)(jB)}\,{}^{B}\boldsymbol{\Phi}_{jk} & {}^{E}\tilde{\boldsymbol{k}}_{(jB)(jA)}\,{}^{A}\boldsymbol{\Psi}_{jd} & {}^{E}\tilde{\boldsymbol{k}}_{(jB)(jB)}\,{}^{B}\boldsymbol{\Psi}_{jd}+\boldsymbol{I} \end{bmatrix} \times \begin{bmatrix} {}^{A}\boldsymbol{p}_k & {}^{B}\boldsymbol{p}_k & {}^{A}\boldsymbol{f}_j & {}^{B}\boldsymbol{f}_j \end{bmatrix}^{\mathrm{T}} = \begin{bmatrix} \boldsymbol{C}_{kk} & \boldsymbol{C}_{dd} \end{bmatrix} \begin{Bmatrix} \boldsymbol{p}_k \\ \boldsymbol{f}_j \end{Bmatrix} = \boldsymbol{0} \quad (16)$$

Then

$$\begin{bmatrix} {}^{A}\boldsymbol{p}_k & {}^{B}\boldsymbol{p}_k & {}^{A}\boldsymbol{f}_j & {}^{B}\boldsymbol{f}_j \end{bmatrix}^{\mathrm{T}} = \begin{bmatrix} \boldsymbol{I} \\ -\boldsymbol{C}_{dd}^{-1}\boldsymbol{C}_{kk} \end{bmatrix} \begin{Bmatrix} {}^{A}\boldsymbol{p}_k \\ {}^{B}\boldsymbol{p}_k \end{Bmatrix} = \boldsymbol{T}_3 \begin{Bmatrix} {}^{A}\boldsymbol{p}_k \\ {}^{B}\boldsymbol{p}_k \end{Bmatrix} \quad (17)$$

Thus one can obtain the second coordinates transformation

$$\begin{Bmatrix} {}^{\mathrm{A}}\boldsymbol{p}_k \\ {}^{\mathrm{A}}\boldsymbol{f}_j \\ {}^{\mathrm{E}}\boldsymbol{u}_{jA} \\ {}^{\mathrm{E}}\boldsymbol{u}_{jB} \\ {}^{\mathrm{B}}\boldsymbol{p}_k \\ {}^{\mathrm{B}}\boldsymbol{f}_j \end{Bmatrix} = \begin{bmatrix} \boldsymbol{I} & \boldsymbol{0} & \boldsymbol{0} & \boldsymbol{0} \\ \boldsymbol{0} & \boldsymbol{0} & \boldsymbol{I} & \boldsymbol{0} \\ {}^{\mathrm{A}}\boldsymbol{\Phi}_{jk} & \boldsymbol{0} & {}^{\mathrm{A}}\boldsymbol{\Psi}_{jd} & \boldsymbol{0} \\ \boldsymbol{0} & {}^{\mathrm{B}}\boldsymbol{\Phi}_{jk} & \boldsymbol{0} & {}^{\mathrm{B}}\boldsymbol{\Psi}_{jd} \\ \boldsymbol{0} & \boldsymbol{I} & \boldsymbol{0} & \boldsymbol{0} \\ \boldsymbol{0} & \boldsymbol{0} & \boldsymbol{0} & \boldsymbol{I} \end{bmatrix} \times \begin{bmatrix} \boldsymbol{I} \\ -\boldsymbol{C}_{dd}^{-1}\boldsymbol{C}_{kk} \end{bmatrix} \begin{Bmatrix} {}^{\mathrm{A}}\boldsymbol{p}_k \\ {}^{\mathrm{B}}\boldsymbol{p}_k \end{Bmatrix} = \boldsymbol{T}_2\boldsymbol{T}_3 \begin{Bmatrix} {}^{\mathrm{A}}\boldsymbol{p}_k \\ {}^{\mathrm{B}}\boldsymbol{p}_k \end{Bmatrix} = \boldsymbol{T} \begin{Bmatrix} {}^{\mathrm{A}}\boldsymbol{p}_k \\ {}^{\mathrm{B}}\boldsymbol{p}_k \end{Bmatrix} \quad (18)$$

Substituting Equation (18) into Equation (8), one can obtain system's equation of free vibration under the approximate space of generalized coordinate $\boldsymbol{q} = \begin{bmatrix} {}^{A}\boldsymbol{p}_k & {}^{B}\boldsymbol{p}_k \end{bmatrix}^{\mathrm{T}}$, which is given by

$$\boldsymbol{M}\ddot{\boldsymbol{q}} + \boldsymbol{K}\boldsymbol{q} = \boldsymbol{0} \quad (19)$$

Where,

$$\boldsymbol{M} = \boldsymbol{T}^{\mathrm{T}}\boldsymbol{m}\boldsymbol{T} \quad \boldsymbol{K} = \boldsymbol{T}^{\mathrm{T}}\boldsymbol{k}\boldsymbol{T} \quad (20a)(20b)$$

2.4 Inverse transform to physical coordinates

For free-interface substructure,

$$\boldsymbol{u} = \begin{bmatrix} {}^{\mathrm{A}}\boldsymbol{u} & {}^{\mathrm{B}}\boldsymbol{u} \end{bmatrix}^{\mathrm{T}} = \boldsymbol{T}_4\boldsymbol{T}_3\boldsymbol{q} \quad (21)$$

Where

$$\boldsymbol{T}_4 = \begin{bmatrix} {}^{\mathrm{A}}\boldsymbol{\Phi}_{ik} & {}^{\mathrm{B}}\boldsymbol{\Phi}_{ik} & {}^{\mathrm{A}}\boldsymbol{\Phi}_{jk} & {}^{\mathrm{B}}\boldsymbol{\Phi}_{jk} \\ {}^{\mathrm{A}}\boldsymbol{\Psi}_{id} & {}^{\mathrm{B}}\boldsymbol{\Psi}_{id} & {}^{\mathrm{A}}\boldsymbol{\Psi}_{jd} & {}^{\mathrm{B}}\boldsymbol{\Psi}_{jd} \end{bmatrix}^{\mathrm{T}} \quad (22)$$

For super-element link substructure,

$${}^{E}\boldsymbol{u} = {}^{E}\boldsymbol{\Psi}_c\boldsymbol{T}_1\boldsymbol{T}_3\boldsymbol{q} \quad (23)$$

The derivation can also be done by dynamic condensation, which will lead to an iterative solving calculation for nonlinear eigenvalue problem, thus the computational efficiency is influenced.

2.5 Summary

Whether in static condensation or dynamic condensation, the super-element indirect CMS deduced by this paper will eventually solve system's dynamic problem in the approximate space which is set out by the normal mode coordinates of every free-interface substructure, which reduces system's DOFs enormously. Because the generalized coordinates of link substructure don't take part in constructing approximate solving space. In that case, when there are non-linear elements in link substructure, we only need to modify the coordinate transformation matrix to modify system's generalized *k*, *c* and *m* matrix. Therefore, the computational efficiency improves.

On the other hand, the introduction of super-element link substructure can handle components' structural damping and connectors' lumped damping separately and then couple into the entire system, which is better than Raleigh damping, especially for some devices with concentrated damping such as rubber bearings, dampers and so on.

3. Application: modal analysis of a truss bridge in ACT

3.1 Brief introduction to the truss bridge

In existing ACT, it usually uses automatic guided vehicles (AGV) or container trucks to transport containers between container cranes and yard. But both of them have the same problems: high cost and low efficiency. As shown in Figure 2, a creative plan of truss bridge between container cranes and the yard to transport containers by electric vehicles has been proposed to solve the problem.

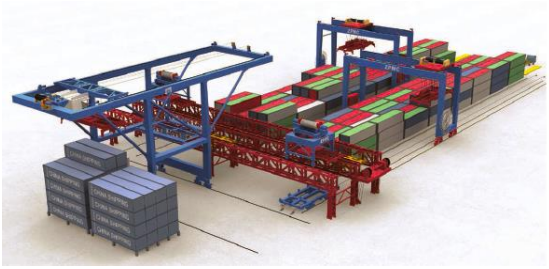

Figure 2. Virtual reality simulation for the automated container terminal experimentation

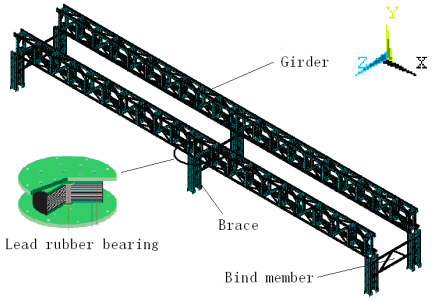

Figure 3. Structure sketch map of the truss bridge

The truss bridge (as shown in Figure 3) mainly consists of trussed girder, braces, and bind members *etc*. The girder and the braces either have rigid connection or are LRB linked.

LRB is a common device for seismic isolation and energy consumption, and widely used in bridges and constructions for its merits of simple structure, easy manufacture, and convenient installation and so on. Because of LRB's complicated non-linear characteristic, researchers usually adopt the equivalent linear model or the bilinear model in current analysis or design [9]. According to the equivalent linear model, mechanical characteristic parameters of the LRB are listed in Table 1.

Table 1. Characteristic parameters of the LRB

Type	Mass m (kg)	Vertical Stiffness K_v (N/m)	Equivalent Horizontal Stiffness k_B (N/m)
GZY500	228	1.972×10^9	1.91×10^6

3.2 Comparative analysis of the truss bridge's natural characteristic

Regarding the LRB as link substructure, girder, brace, bind member as free-interface substructures (fetch the first 30 orders of modes), respectively apply the dual-coordinate free interface CMS method and super-element indirect CMS to analyze natural characteristic of the truss bridge. Frequency (Hz) results (first 20 orders) comparison of the truss bridge rigid linked or LRB linked follows in Table 2, and use finite element method for precise construed error analysis. Parts of the modes are shown in Figure 4.

Table 2. Natural frequency (Hz) results comparison of the truss bridge rigid or LRB linked

Order	Rigid linked			LRB Linked		
	FEM	Free Interface CMS	Error /%	FEM	Indirect CMS	Error /%
1	2.4198	2.4198	0.00	1.3669	1.3769	0.73
5	3.1273	3.1273	0.00	1.5969	1.6201	1.45
10	5.2353	5.2353	0.00	3.4900	3.5790	2.55
15	7.2827	7.2830	0.01	6.0457	6.2277	3.01
20	7.8941	7.9052	0.14	7.2864	7.5363	3.43

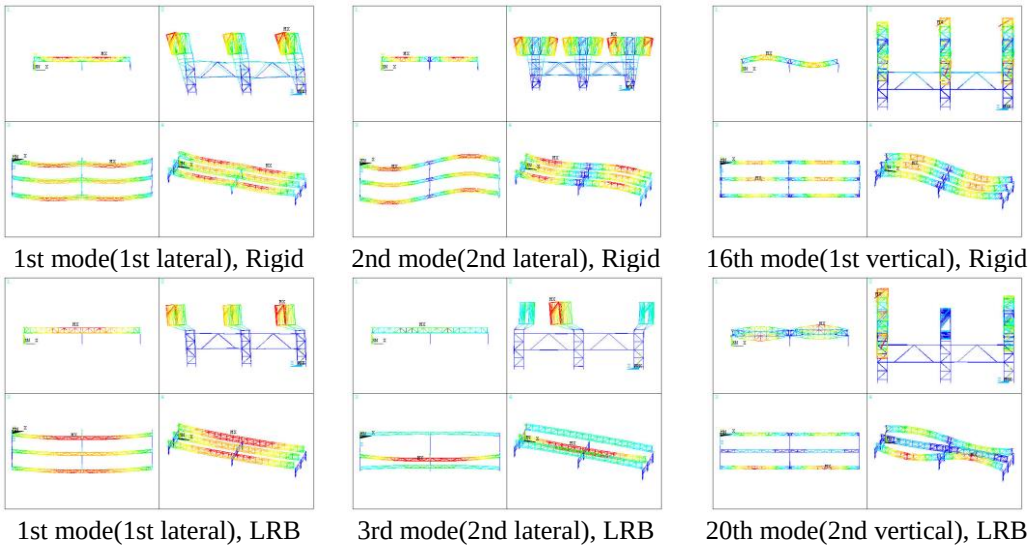

1st mode(1st lateral), Rigid | 2nd mode(2nd lateral), Rigid | 16th mode(1st vertical), Rigid

1st mode(1st lateral), LRB | 3rd mode(2nd lateral), LRB | 20th mode(2nd vertical), LRB

Figure 4. Simulation modes of the truss bridge rigid or LRB linked

According to Table 2: (1) LRB reduced the natural frequency of the truss bridge greatly. The natural frequency of the first 10 rigid support modes is 1.5 to 2 times larger than that LRB linked. Using LRB can be a way of structure frequency modulation. (2) The dual-coordinate free interface CMS method has high natural frequency calculation accuracy. The accuracy of the proposed super-element indirect CMS is also high, and the maximum error of the first 20 orders is less than 4%.

4. Structural model test validation

4.1 Structural dynamic modal similarity principle and model test design

Take Force, Length and Time as fundamental dimension system ([F, L, T]), structural dynamic similarity principles can be derived by dimensional analysis. Similar relationships with respect to the inherent characteristics of the main physical quantities are listed in Table 3. Other physical quantities such as area *A*, volume *V* and frequency *f* can be derived from the similar relationships of length *l* and time (period) *T*. After considering the economic, test conditions and other factors, the geometric similarity constant of the model can be determined as c_l=1/30; the material of the model is the same as prototype so that c_E=1; thus, the similar constants (model/prototype) are determined in Table 3 according to the similar relationships.

Table 3. Similarity principle with respect to inherent characteristics structural model test

Physical Quantities	Dimension	Similar Relationship	Similar Constant
Length *l*	[L]	c_l	1/30
Mass *m*	$[FL^{-1}T^2]$	$c_m = c_r c_l^3$	$1/30^2$
Stiffness *k*	$[FL^{-1}]$	$c_k=c_E c_l$	1/30
Damping *c*	$[FL^{-1}T]$	$c_c=c_E c_l^{3/2}$	$1/30^{3/2}$
Elastic modulus *E*	$[FL^{-2}]$	c_E	1
Density *r*	$[FL^{-4}T^2]$	$c_r = c_E / c_l$	30
Time (Period) *T*	[T]	$c_t=c_l^{1/2}$	$1/\sqrt{30}$

Add equable weight to approximately satisfy the similar constant $c_r = 30$. And in the model design, section area and section inertia moment comply with associated value in Table 3. Use circular rubber spring plus central lead to simulate LRB. Lower order natural frequency error of prototype simulation and the model test do not reach up 10%. The designed model is shown in Figure 5.

Figure 5. Photos of the truss bridge and the LRB model

4.2 Test method and instrumentation

Measure the inherent characteristics through hammer and MISO method. Test equipments are shown in Figure 6 as follows: (1) KISTLER 9722A2000-type of hammer exciter; (2) KISTLER 8632C50-type of acceleration sensor; (3) Analyzer AZ116-type of signal acquisition system; (4) KISTLER 5 134-type of voltage amplifier; (5) CRAS V6.1-type of vibration and dynamic signal acquisition and analysis system as analysis software.

(1) (2) (3) (4) (5)

Figure 6. Modal test equipment and software

4.3 Comparison between model test and prototype simulation results

The comparison between the low-order natural frequency results of model test and prototype simulation in the lateral (z) and vertical (y) direction, when the truss bridge is rigid or LRB linked, is shown in Table 4.

From Table 4, the natural frequency results of model test are near to the prototype simulation results, no matter the truss bridge is rigid linked or LRB linked. The main reasons for slightly larger error of LRB linked are: the existence of gap between the rubber spring and the positioning ring (in Figure 5) and the nonlinearity of rubber material. The test modes and the simulated modes also agree well.

Table 4. Natural frequency (Hz) results comparison of model test and prototype simulation

Rigid Linked				LRB Linked			
Order	**Simulation**	**Test**	**Error**	**Order**	**Simulation**	**Test**	**Error**
1(1st lateral)	2.42	12.4	6.2%	1(1st lateral)	1.37	6.8	9.4%
2(2nd lateral)	2.80	14.5	5.7%	2(2nd lateral)	1.41	7.1	8.5%
3(3rd lateral)	2.93	17.0	6.1%	3(3rd lateral)	1.43	8.3	6.0%
4(4th lateral)	2.98	17.2	5.0%	4(4th lateral)	1.96	11.9	10.9%
16(1st vertical)	7.57	38.7	6.6%	19(1st vertical)	7.29	36.1	9.5%
17(2nd vertical)	7.65	40.4	3.5%	20(2nd vertical)	7.30	37.8	5.3%

Note: Before the error calculation, the model test results should be divided by the similar constant $\sqrt{30}$.

5. Conclusion

(1) Based on the free-interface component mode synthesis (CMS) method, the inherent characteristics of a truss bridge in Automated Container Terminal, either rigid support or LRB linked, are analyzed and compared. The results show the LRB's obvious effect on frequency modulation for the truss bridge.

(2) Deduced a new technique of indirect free-interface CMS (referred to as super-element indirect CMS) by Guyan static condensation, which can reduce system DOFs greatly and has

high calculation accuracy. The proposed technique is particularly suitable for system dynamic analysis with nonlinear substructures such as the LRB, nonlinear spring, etc.

(3) The results of model test and prototype simulation prove with each other, that the simulation results and the test design are reliable, also validates the proposed CMS technique and the LRB's effect on frequency modulation.

Acknowledgements

This work is sponsored by Shanghai Top Academic Discipline Project- Management Science & Engineering, Shanghai Education Committee Project "Shanghai Young College Teacher Training Subsidy Scheme"(shs11023), this paper is supported by Science & Technology Program of Shanghai Maritime University(20110041), also supported in part by National Natural Science Foundation project(71101090), Ministry of Transport Research Projects (2012-329-810-180), Shanghai Municipal Education Commission Project (12ZZ148, 13YZ080).

References

[1] Y. Xia, "Substructure mode synthesis methods for dynamic analysis of payloads and launch vehicle interaction", Structure & Environment Engineering, vol. 4, **(1996)**, pp. 36-42.
[2] C. Zou, D. Chen and H. Hua, "Modal synthesis method of structural vibration analysis of ship", Journal of Shanghai Jiaotong University, vol. 37, **(2003)**, pp. 1213-1218.
[3] M. Fang and Q. Feng, "Vibration analysis of automobile dynamical system with nonlinearity", Journal of Tongji University (Natural Science), vol. 35, **(2007)**, pp. 1524-1528.
[4] S. Xiang, J. Qiu and D. Wang, "The resent progresses on modal analysis and dynamic sub-structure methods", Advances in Mechanics, vol. 34, **(2004)**, pp. 289-303.
[5] M. Lou, "A new modal synthesis technique for mixed-interface substructures with link area", Chinese Journal of Computational Mechanics, vol. 11, **(1994)**, pp. 306-313.
[6] M. Lou, "Link substructure and modal synthesis for substructuring", Journal of Vibration Engineering, vol. 8, **(1995)**, pp. 52-56.
[7] Y. Wang, "Theory and application of dynamic substructure methods", Science Press, Beijing, **(1999)**.
[8] K. Lu, H. Qiu and Z. Gui, "Analysis on structural buckling and local stability for truss low bridge of automated container terminal", Chinese Journal of Construction Machinery, vol. 6, **(2008)**, pp. 287-292.
[9] L. Fan and Z. Wang, "Seismic isolation design for bridges", China Communications Press, Beijing, **(2001)**.
[10] J. Yang, "Similarity principle and structural model test", Wuhan University of Technology Press, Wuhan **(2005)**.

Authors

LU Kai-liang, received his PhD from Tongji University, Shanghai, China. Currently, he is working in Logistics Engineering College, Shanghai Maritime University (SMU) as a lecturer. His research interests include port machine structure and system dynamics, theory and method of dynamic design and optimization of structure, etc. He has 12 publications to his credit both in international and national Journals. He is a committee member of Shanghai Society of Theoretical & Applied Mechanics, member of China Construction Machinery Society (CCMS), and Logistics Engineering Institution, CMES.

YAN Wei, received his PhD from Nanyang Technological University (NTU), Singapore. Currently, He is working as the director of Development Planning Division, SMU and the deputy director of Engineering Research Center for Container Supply Chain Technology, MOE, China. He has been entitled as the committee member of the Shanghai Shuguang Scholar, etc. He completed 1 state-key textbook, over 10 patents, and more than 100 publications, including over 30 SCI/SSCI-indexed papers as well as more than 250 SCI citations.

DING Qiu-yi, major in Mechanical and Electrical Engineering (Sino-Dutch joint program), second year student of Logistics Engineering College, SMU. At present, she is a member of a college student's scientific innovation project of Shanghai Education Committee.

WANG Chao, major in Mechanical and Electrical Engineering (Sino-Dutch joint program), second year student of Logistics Engineering College, SMU. At present, he is the team-leader of a college student's scientific innovation project of Shanghai Education Committee.